Vehicle Front-End Architecture as a Driving Factor in Occupant Injury Risk During Vehicle-Guardrail Impacts: A Hybrid III Dummy-Based Numerical Study

Maheep Bubna[1], Elijah Buckland[1], Dr. Luke E. Riexinger[2], Dr. Costin Untaroiu[3]
[1] Department of Mechanical Engineering, Virginia Tech, Blacksburg, VA, USA; [2] Insurance Institute for Highway Safety, Ruckersville, VA, USA; [3] Department of Biomedical Engineering, Virginia Tech, Blacksburg, VA, USA

ABSTRACT

The performance of Midwest Guardrail Systems (MGS) during impact with electric vehicles (EV) has raised concerns with recent observations demonstrating a higher susceptibility to rail-failures. These failures are hypothesized to be related to EV-specific design, including variations in front-end geometry and inertial properties. Current guardrail evaluations rely on two vehicle types, a small car and a pickup truck, potentially overlooking sensitivity to front-end geometry variations, potentially leading to unanticipated impact responses. Additionally, the extent to which geometry influences occupant injury risks and trends during vehicle guardrail impact remains insufficiently investigated. The objective of this study is to quantify the influence of vehicle front-end geometry on occupant injury risk during vehicle-guardrail impacts using Finite Element (FE) simulations. Occupant injury risk is analyzed using Hybrid III dummy-based injury criteria and flail space-based vehicle severity metrics to identify trends and relationship between geometric variations and injury probability. Front end geometry data from the Insurance Institute of Highway Safety (IIHS) was analyzed to identify parameters and ranges associated with adverse MGS performance. Based on vehicle alignment with the w-beam, hood leading edge height, hood leading edge angle, and bumper height were morphed on the Toyota Yaris model. A Latin Hypercube Design of Experiments generated 13 unique configurations for detailed analysis. Full scale Manual for Assessing Safety Hardware (MASH) Test Level 3 FE simulations were then performed between the morphed vehicle models integrated with Hybrid III 50th percentile male dummy and MGS guardrail. Occupant injury metrics were evaluated alongside vehicle-based crash severity measures. All vehicle geometries fulfilled MASH criteria with occupant impact velocity (OIV) and occupant ride down acceleration (ORA) within tolerance with no rail rupture. Simulations suggest that probability of serious full-body injury (AIS3+) was estimated at 17.11% while probability of severe neck injury was the highest at 15.64% amongst the component level probabilities. While front-end geometry influences occupant kinematics, resulting injury metrics and vehicle-guardrail interaction characteristics, it does not independently govern occupant injury risk. Although, the MASH tests have the same outcome as the geometries studied, the changes in EV inertial properties could interact with the geometry leading to barrier failure, which will be explored in future work.

This paper is a student paper from the 21st Injury Biomechanics Symposium and is published in a special issue of SAE International Journal of Transportation Safety.
It is preliminary work, has not been peer reviewed, and should not be cited because it is a work in progress.

INTRODUCTION

The increasing popularity and adoption of electric vehicles (EVs) has introduced new challenges for roadside safety hardware. The Midwest Roadside Safety Facility's (MwRSF) recent crash testing demonstrated that EVs can interact with the Midwest Guardrail System (MGS) differently than comparable internal combustion engine vehicles (ICEV) (Bielenberg et al., 2026). The Tesla Model 3 underwent complete barrier underride, while the Rivian R1T ruptured the rail. Although the contributing mechanisms responsible for these failures are under-researched, proposed causes include higher vehicle mass, lower center of gravity (CG) height, higher structural stiffness and variations in front-end geometry associated with EV architecture (Bielenberg et al., 2026). Consequently, it is vital to research whether front-end geometry influences vehicle-to-barrier impact outcome for any vehicle. Roadside safety hardware testing in the United States is performed according to the Manual for Assessing Safety Hardware (MASH) (AASHTO, 2016). Under Test Level 3 (TL-3) conditions, longitudinal barriers such as the MGS are evaluated using two vehicles, a 1,100 kg small sedan and a 2,270 kg pickup truck. The pickup truck assesses barrier structural adequacy, while the small car evaluates occupant risk during redirection. However, these vehicles may not represent the whole range of front-end geometries found in conventional ICEVs and modern EVs.

MASH injury criteria relies on the flail space model (FSM) to assess occupant risk, which does not provide body-region-specific injury information (AASHTO, 2016). Since front-end geometry can influence vehicle underride (Ferdous et al., 2011; Julin et al., 2012; Marzougui et al., 2007), occupant kinematics and compartment intrusion (Eigen & Glassbrenner, 2004) understanding its effect is important for evaluating occupant safety. Previous studies have shown that occupant compartment intrusion is strongly associated with injury severity (Eigen & Glassbrenner, 2004), and EVs may experience greater frontal deformation due to the absence of a conventional engine block (Żuchowski, 2018). Therefore, understanding the influence of front-end geometry i.e., geometries outside the standard MASH test vehicles on crash response is important for assessing occupant safety performance.

Previous studies have investigated effects of parameters such as increased mass, lower CG and increased chassis stiffness (Storozhev & Vafaeva, 2025; Yücel, 2024). Other studies found that higher guardrail mounting heights can increase the likelihood of vehicle underride (Julin et al., 2012) highlighting the importance of vehicle-to-barrier geometric interaction. However, the influence of specific front-end geometric parameters such as hood leading-edge angle, bumper height, and ground clearance has not been investigated.

The objective of this study is to investigate the influence of front-end geometry on occupant injury outcomes and compare them to vehicle-based crash severity metrics during vehicle-to-MGS impacts under MASH TL-3 conditions. Full body and component-level driver injury probabilities for a Hybrid III 50th percentile male dummy are evaluated, and the influence of geometric parameters on injury response is analyzed. In addition, injury predictions obtained using the Flail Space Model (FSM) and EN1317 vehicle-based crash severity metrics are compared.

This paper is a student paper from the 21st Injury Biomechanics Symposium and is published in a special issue of SAE International Journal of Transportation Safety.
It is preliminary work, has not been peer reviewed, and should not be cited because it is a work in progress.

METHODS

Front-End Geometry Parametrization and Simulation Setup

Congruent with observations from the Tesla Model 3 MGS test (Bielenberg et al., 2026), vehicles with lower hood leading edge heights and bumper heights were hypothesized more susceptible to underride, while smaller hood leading angles were associated with increased likelihood of the rail to rising-up over the fender and hood (Julin et al., 2012). Front-end geometry data, including hood leading edge height, hood leading edge angle, hood angle, bumper height, and ground clearance was collected for 2,958 vehicles (model year 2011 and newer) comparable to MASH small car using the IIHS database (Hu et al., 2024). Parameters were screened and identified based on alignment with the 31" MGS W-beam guardrail profile and their potential to contribute to adverse vehicle-barrier interactions observed in recent crash testing. Based on this screening, hood leading edge height, hood leading edge angle, and bumper height were selected as primary variables while, the remaining parameters were held constant (Fig. 1). Parameter bounds were based on values associated with adverse interaction conditions, while ensuring feasibility within production vehicles through percentile-based distribution data (sales volume) (Table 1). Although some parameter values may seem extreme such as hood leading edge height, they are consistent with dimensions observed in best-selling EVs in the United States market, including the Tesla Model 3 (Liu et al., 2025).

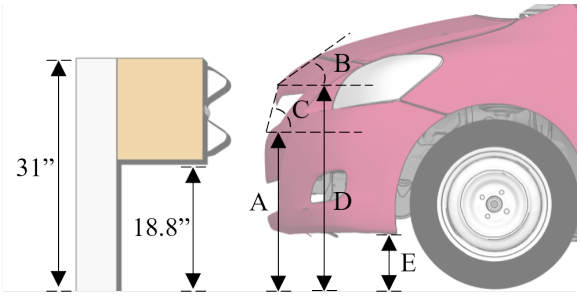

Figure 1: Vehicle front-end geometry nomenclature and relative standing against a 31" MGS installation. (A) Hood leading Edge Height; (B)Hood Angle; (C) Hood Leading Edge Angle; (D) Bumper Height; (E) Ground Clearance.

Table 1: Design of Experiment - Factors and Levels

Vehicle	Factor	Levels		
		1	2	3
1100C Small Car (Toyota Yaris)	Hood leading edge height *cm(in), percentile*	63.5 (25) [P3]	76.2 (30) [P62]	81.3 (32) [P85]
	Hood leading edge angle, *percentile*	50° [P4]	65° [P51]	80° [P82]
	Bumper height *cm(in), percentile*	38.1 (15) [P9]	52.8 (20.8) [P51]	55.9 (22) [P74]

This paper is a student paper from the 21st Injury Biomechanics Symposium and is published in a special issue of SAE International Journal of Transportation Safety.
It is preliminary work, has not been peer reviewed, and should not be cited because it is a work in progress.

A total of 13 design configurations were developed using a Latin Hypercube (LH) Design of Experiment (DOE) in LS-OPT, ensuring computational efficiency and statistical robustness for global sensitivity analysis. A previously validated detailed Finite Element (FE) model of the Toyota Yaris (MASH small car) with a test inertial mass of 1,100kg, developed by the Center for Collision Safety and Analysis (GMU CCSA) (Ferdous et al., 2011; Julin et al., 2012; Meng et al., 2026) was used as the baseline (Fig. 2). The vehicle interior, including the steering wheel and driver seat, was modelled in detail and passive safety systems namely, driver seatbelt and steering-airbag were integrated into the car model. Geometric, material and functional parameters (e.g., seatbelt pretensioner/retractor load curves, and airbag input mass flow rate) were adopted from prior studies (Gandikota et al., 2015; Kang et al., 2018; Masiá et al., 2008). A Hybrid III 50th percentile male dummy was positioned in the driver seat using dummy settling pre-simulation procedure (Fig. 3) (Masiá et al., 2008; Noureddine et al., 2002). The stabilized dummy position, including the H-point and deformed seat cushion geometry was extracted and used as the initial conditions for crash simulations. Subsequently, seat belt routing was refined to ensure proper fit and minimize the risk of submarining. A FE model of the steel post MGS W-beam guardrail (78.7 cm [31 in]) with wooden blockouts (30.5 cm [12 in]), developed by Midwest Roadside Safety Facility, was incorporated (Julin et al., 2012; Polivka et al., 2004). The W-beam splice bolts were modelled to facilitate W-beam separation while a W-beam GISSMO material model was adopted from literature (Alomari et al., 2025). Full-scale simulations were performed in accordance with MASH Test Level-3 (TL-3) procedures for test 3-10 (Fig. 2).

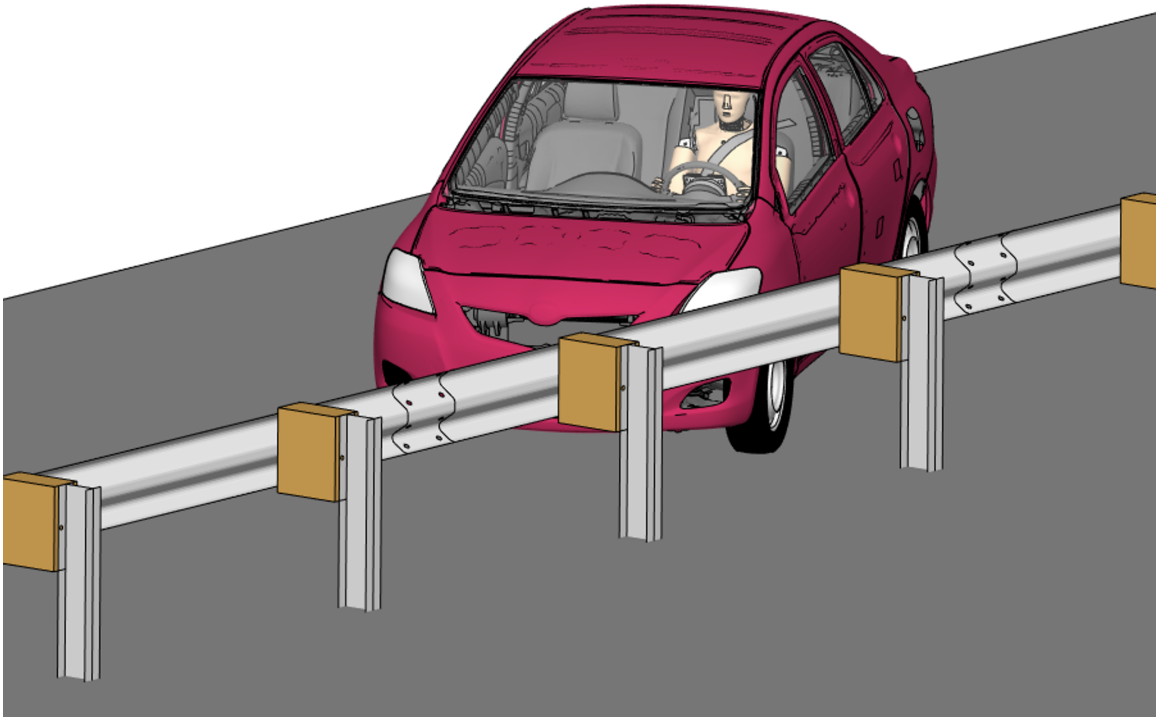

Figure 2: Vehicle to MGS barrier crash setup.

This paper is a student paper from the 21st Injury Biomechanics Symposium and is published in a special issue of SAE International Journal of Transportation Safety.
It is preliminary work, has not been peer reviewed, and should not be cited because it is a work in progress.

Figure 3: Initial positioning of the FE dummy in the driver seat configuration.

Although FE simulation has become a widely accepted tool for roadside safety research, publicly available EV FE vehicle models suitable for MASH TL-3 evaluation remain limited, particularly within the 1,100 kg small-car and 2,270 kg pickup-truck categories used for longitudinal barrier testing. As a result, direct investigation of EV-specific barrier interaction behaviour under standardized roadside safety conditions is currently restricted. Previous roadside safety and crashworthiness studies have demonstrated the use of validated FE vehicle models for evaluating non-standard impact conditions, geometric variations, and parametric design changes (Ray, 1997; Pernetti et al., 2007). Similarly, recent vehicle safety studies have employed geometric morphing and parametric modification techniques to investigate the influence of front-end geometry on crash response and injury outcomes when representative vehicle models were unavailable (Hu et al., 2023). Following this approach, the present study applies controlled geometric morphing to a validated MASH 1100C FE vehicle model to represent a range of front-end geometries. While the modified models do not fully replicate EV structural architecture, the methodology enables isolation and evaluation of the influence of front-end geometric parameters on vehicle-to-barrier interaction, occupant kinematics, and injury response.

The baseline vehicle model was validated against physical test data (Polivka et al., 2006; Polivka et al., 2004) in accordance with NCHRP Report 179 (Ray et al., 2011). Hourglass energy was maintained below 5% of total energy to ensure accurate representation of the physical response. Following validation, the vehicle model was morphed using ANSA (Beta CAE Systems, USA, MI) pre-processing software. Control points at key landmark locations were morphed to achieve desired geometric configurations while maintaining mesh quality and avoiding distortion. The longitudinal chassis members were modified with gradual geometric transitions to avoid discontinuities that could introduce instabilities under crash loading. The modified vehicle models were evaluated using IIHS small-overlap front barrier crash test. Results confirmed that the

This paper is a student paper from the 21st Injury Biomechanics Symposium and is published in a special issue of SAE International Journal of Transportation Safety.
It is preliminary work, has not been peer reviewed, and should not be cited because it is a work in progress.

geometric modifications did not adversely affect chassis structural integrity. To avoid non-physical behaviour, selected components were excluded from the morphing region, including suspension system, rotating components and spotweld connections.

Dummy-Based Crash Severity for Occupant Injury Assessment

For each configuration, impact response of the Hybrid III dummy was monitored and occupant injury risks were extracted, including Head Injury Criteria (HIC), N_{ij} for the neck, maximum chest deflection (at sternum with respect to thoracic spine), chest acceleration (on thoracic spine), and maximum femur load for thigh. These injury metrics were contrasted against the FMVSS 208 injury thresholds (NHTSA, 2023), established for a mid-size male in frontal crashes (Table 2) (Kuppa et al., 2000; Nason, 2007). The probability of sustaining a serious injury (AIS 3+) was estimated on both the body-region and whole-body levels using established injury risk functions (Eq. 1-5) (Cassatta et al., 2013; Eppinger et al., 2000; Gennarelli & Wodzin, 2006).

Table 2: Dummy-based injury criteria and threshold values

Components	Injury criteria	Limits	Source
Head	HIC_{36} HIC_{15}	1000 700	(Bandak et al., 1999; NHTSA, 2023)
Neck	N_{ij}	1	
Thoracic	Chest Deflection (D) Chest Acceleration (A_s)	63mm 60g	
Thigh	Femur Load	10kN	

The probability of head injury (Bandak et al., 1999) is calculated as

$$P_{head} = \Phi\left(\frac{\ln(HIC_{15}) - 7.45231}{0.73998}\right) \quad (1)$$

The probability of neck injury (Bandak et al., 1999) is calculated as

$$P_{neck} = \frac{1}{1 + e^{3.227 - 1.969 \times N_{ij}}} \quad (2)$$

The probability of combined thoracic injury (Bandak et al., 1999) is calculated as

$$P_{chest} = \frac{1}{1 + e^{-(-7.125 + 0.08 \times A_s + 0.064 \times Deflection_{Chest})}} \quad (3)$$

The probability of femur injury (Kuppa et al., 2001) is calculated as

$$P_{femur} = \frac{1}{1 + e^{4.9795 - 0.326 \times F}} \quad (4)$$

This paper is a student paper from the 21st Injury Biomechanics Symposium and is published in a special issue of SAE International Journal of Transportation Safety.
It is preliminary work, has not been peer reviewed, and should not be cited because it is a work in progress.

For the Hybrid III 50th percentile male dummy, the combined probability of at least one AIS3+ injury (Kuppa et al., 2001) is calculated as

$$P(AIS\ 3+) = 1 - \left[(1 - P_{head}) \times (1 - P_{neck}) \times (1 - P_{chest}) \times (1 - P_{femur})\right] \quad (5)$$

Vehicle-Based Crash Severity for Occupant Injury Assessment

Three vehicle-based crash severity metrices were used and compared to predict occupant injury in the crash tests with MGS roadside safety hardware namely, flail space model, ASI and THIV. Flail Space model, the US criteria which was developed for unbelted occupants assumes that the injuries are related to impacts against the vehicle interior parts (AASHTO, 2016). The unbelted point mass occupant is allowed to flail 0.6m longitudinally and 0.3m laterally into the vehicle interior space (Michie, 1981). The flail distance $(\mathrm{d}_x, \mathrm{d}_y)$ are calculated using longitudinal and lateral accelerations of the vehicle centre of gravity as follows:

$$d_i = \int_0^t \int_0^t a_i \, dt^2 \quad (6)$$

Then the occupant impact velocities (OIVs) are calculated as

$$OIV_i = \int_0^{t'} a_i dt \quad (7)$$

Where the timestamp (t') was calculated when either longitudinal displacement (d_x) = 0.6m or lateral displacement (d_y) = 0.3m was reached. The occupant ridedown accelerations (ORA) were computed as the peak 10-ms moving average vehicle acceleration occurring after time (t') using (Eq. 8). The recommended thresholds for OIV and ORA are 12.2 m/s and 20.49g respectively (AASHTO, 2016).

$$ORA = max\left[\frac{1}{0.010}\int_T^{T+0.010} a_i dt\right] for\ all\ T > t' \quad (8)$$

Acceleration Severity Index (ASI), the European standard metric (CEN, 2010a, 2010c) developed for belted occupants was calculated based on accelerations of the vehicle center of gravity (Eq. 9).

$$ASI = \max\left[\sqrt{\left[\frac{\overline{a_x}}{\widehat{a_x}}\right]^2 + \left[\frac{\overline{a_y}}{\widehat{a_y}}\right]^2 + \left[\frac{\overline{a_z}}{\widehat{a_z}}\right]^2}\right] \quad (9)$$

Where acceleration $\overline{a_i}$ was filtered using a CFC 180 filter compliant with ISO 6487 (CEN, 2010b). The corresponding limit acceleration values $\widehat{a_i}$ were defined as 12g, 9g and 10g in x, y and z directions, respectively. To ensure valid comparison between MASH and EN 1317 guidelines, the ASI threshold of 1.9 or severity level C was adopted in this study. Because the EN1317 guideline is based on a lighter vehicle (900 kg) compared to the small car (1,100 kg), the highest severity value was selected.

This paper is a student paper from the 21st Injury Biomechanics Symposium and is published in a special issue of SAE International Journal of Transportation Safety.
It is preliminary work, has not been peer reviewed, and should not be cited because it is a work in progress.

Theoretical Head Impact Velocity (THIV) is another safety performance metric commonly used in roadside barrier testing standards such as EN 1317 and was calculated using (Eq. 10-13) (CEN, 2010c). As per EN 1317 guidelines, the limiting THIV for lateral impacts in MASH TL3 crash test was defined as less than or equal to 33 km/h (CEN, 2010b).

$$\ddot{X}_c = a_x \cos\Psi - a_y \sin\Psi$$
$$\ddot{Y}_b = a_x \sin\Psi - a_y \cos\Psi \quad (10)$$

$$x_b = (x_0 - X_c)\cos\Psi - (y_0 - Y_c)\sin\Psi$$
$$y_b = -(x_0 - X_c)\sin\Psi + (y_0 - Y_c)\cos\Psi \quad (11)$$

$$\dot{x_b} = -\dot{X_c}\cos\Psi - \dot{Y_c}\sin\Psi + y_b\dot{\Psi}$$
$$\dot{y_b} = -\dot{X_c}\sin\Psi - \dot{Y_c}\cos\Psi + x_b\dot{\Psi} \quad (12)$$

$$THIV = \sqrt{\dot{x_b}(\acute{t})^2 + \dot{y_b}(\acute{t})^2} \quad (13)$$

Where,a_x and a_y represent the longitudinal and lateral vehicle accelerations in the local coordinate system, while Ψ denotes the angle between the guardrail and the vehicle centerline. The time of impact, $\acute{t}$, is defined as the time at which the occupant displacement equals either 0.6 m or 0.3 m in the longitudinal or lateral direction respectively (CEN, 2010c). In the present study, the initial longitudinal distance between the dummy head CG and the vehicle CG (x_0) was measured at the onset of the crash simulation and found to be 0.12 m. The lateral offset (y_0) was assumed to be zero, consistent with the guideline requirements (CEN, 2010c).

Sobol Indices and Correlation Matrix

To determine the most influential geometric parameters affecting injury severity, Sobol's global sensitivity analysis (GSA) was performed using LS-Opt (ANSYS, Canonsburg, USA, PA). This variance-based method provides relative contribution of each input parameter to the variation caused by the interaction of the variable across the domain (Andres et al., 2008). Additionally, a correlation matrix was derived from LS-OPT to assess the direction and degree of influence on the responses. The matrix was based on the Pearson correlation coefficient, which evaluates linear association between variables and responses (Eq. 14) (Pearson, 1895).

$$r_{xy} = \frac{\sum_{k=1}^{N}(x_k - \bar{x})(y_k - \bar{y})}{\sqrt{\sum_{k=1}^{N}(x_k - \bar{x})^2}\sqrt{\sum_{k=1}^{N}(y_k - \bar{y})^2}} \quad (14)$$

Where, x and y represent the normalized design variable and response respectively, on a scale of [-1, +1] and $\bar{x}$ and $\bar{y}$ represent the average values. A coefficient of -1, 0 and 1 represent strong negative, weak or no linear and strong positive association, respectively. The correlation coefficients are free of range bias and parameter scaling as normalization is performed prior to the calculations.

This paper is a student paper from the 21st Injury Biomechanics Symposium and is published in a special issue of SAE International Journal of Transportation Safety.
It is preliminary work, has not been peer reviewed, and should not be cited because it is a work in progress.

RESULTS

Overall, all 13 vehicle configurations satisfied the MASH criteria with OIV and ORA remaining below the prescribed limits. All vehicles were successfully redirected into the crash box. No instances of vehicle rollover, snagging, or structural failure was observed however geometric variations did influence kinematic behavior. The mean longitudinal and lateral OIVs were recorded to be 8.15 m/s and 5.07 m/s, respectively, while the corresponding mean longitudinal and lateral ORAs were 10.38 g and 9.34 g (Table 3). Furthermore, all configurations also fulfilled the European EN1317 criteria. The average ASI and THIV were recorded as 1 and 8.45km/h, respectively (Table 3). The evaluated vehicle configurations also satisfied FMVSS 208 assessment criteria, as all dummy injuries remained under the acceptable limits (Table 4). The mean probability of serious full-body injury (AIS3+) was estimated at 17.114%. The average probabilities of serious injury to the head, neck, chest and femur were 0.013%, 15.64%, 0.598% and 1.142% respectively (Table 5).

Table 3: Vehicle-based crash severity metrics for 1100C Small Car (Toyota Yaris)

Design Point	Hood Leading Edge Height (cm)	Hood Leading Edge Angle (°)	Bumper Height (cm)	Vehicle-Based Crash Severity					
				OIVx (m/s)	OIV_y (m/s)	ORA_x (g)	ORA_y (g)	ASI	THIV
Baseline	71.1	70.1	178.1	9.96	5.18	8.25	7.73	1.07	9.94
DP 01	63.5	50	127.0	6.95	5.41	10.53	8.73	0.91	7.85
DP 02	63.5	65	165.1	7.13	5.20	11.04	8.88	0.96	7.90
DP 03	76.2	65	165.1	9.82	5.12	9.64	9.71	1.01	9.58
DP 04	76.2	50	127.0	7.75	5.14	10.49	9.02	1.00	8.23
DP 05	76.2	50	127.0	8.72	4.74	13.10	9.55	1.15	8.67
DP 06	76.2	80	203.2	7.83	4.95	8.77	10.05	0.93	8.10
DP 07	76.2	80	203.2	7.75	5.49	9.58	11.50	0.95	8.04
DP 08	81.3	65	165.1	10.22	4.66	8.35	7.20	1.07	10.07
DP 09	76.2	80	203.2	8.46	4.95	9.64	9.91	0.92	8.71
DP 10	63.5	80	203.2	7.72	4.69	10.25	9.37	1.07	8.17
DP 11	63.5	65	165.1	7.28	5.02	10.65	10.49	1.04	7.59
DP 12	76.2	65	165.1	7.49	5.29	15.37	8.92	0.99	8.00
DP 13	63.5	65	165.1	6.97	5.11	9.69	9.76	0.99	7.44
Average				8.15	5.07	10.38	9.34	1	8.45
MASH and EN1318 Limits				12.2	12.2	20.49	20.49	1.9	33

This paper is a student paper from the 21st Injury Biomechanics Symposium and is published in a special issue of SAE International Journal of Transportation Safety.
It is preliminary work, has not been peer reviewed, and should not be cited because it is a work in progress.

Table 4: Dummy-based crash severity metrics for 1100C Small Car (Toyota Yaris)

Design Point	Hood Leading Edge Height (cm)	Hood Leading Edge Angle (°)	Bumper Height (cm)	Dummy-Based Crash Severity					
				HIC_{36}	HIC_{15}	N_{ij}	Chest Def. (mm)	Chest Acc (g)	Femur Load (kN)
Baseline	71.1	70.1	178.1	179.62	148.73	0.93	18.48	30.47	1.04
DP 01	63.5	50	127.0	93.39	89.41	0.72	13.83	22.57	0.89
DP 02	63.5	65	165.1	168.76	108.53	0.77	14.02	26.57	0.96
DP 03	76.2	65	165.1	175.24	133.90	0.53	15.06	25.35	2.24
DP 04	76.2	50	127.0	171.19	116.11	0.86	14.68	29.36	1.43
DP 05	76.2	50	127.0	163.18	91.91	0.81	14.74	25.84	2.12
DP 06	76.2	80	203.2	149.96	100.45	0.84	13.92	27.93	1.28
DP 07	76.2	80	203.2	129.10	98.61	0.82	15.15	25.59	1.62
DP 08	81.3	65	165.1	174.46	144.21	1.00	14.13	26.46	2.07
DP 09	76.2	80	203.2	156.32	96.64	0.81	14.95	22.31	1.10
DP 10	63.5	80	203.2	162.93	109.20	0.78	13.37	21.27	1.20
DP 11	63.5	65	165.1	68.52	67.18	0.58	14.96	24.10	3.14
DP 12	76.2	65	165.1	117.93	84.11	0.72	14.74	27.41	1.34
DP 13	63.5	65	165.1	95.48	95.48	0.66	13.70	26.77	0.91
Average				143.29	106.03	0.77	14.69	25.86	1.52
FMVSS 208 Limits				1000	700	1	63	60	10

This paper is a student paper from the 21st Injury Biomechanics Symposium and is published in a special issue of SAE International Journal of Transportation Safety.
It is preliminary work, has not been peer reviewed, and should not be cited because it is a work in progress.

Table 5: Dummy-based crash injury probabilities

Design Point	Hood Leading Edge Height (cm)	Hood Leading Edge Angle (°)	Bumper Height (cm)	Dummy-Based Crash Injury Probabilities				
				P(AIS 3+)	P_{Head}	P_{Neck}	P_{Chest}	P_{Femur}
Baseline	71.1	70.1	178.1	21.613	0.047	19.964	1.070	0.955
DP 01	63.5	50	127.0	15.337	0.003	14.120	0.507	0.912
DP 02	63.5	65	165.1	16.420	0.009	15.181	0.524	0.933
DP 03	76.2	65	165.1	11.880	0.028	10.037	0.625	1.405
DP 04	76.2	50	127.0	19.061	0.013	17.679	0.587	1.085
DP 05	76.2	50	127.0	18.004	0.004	16.382	0.592	1.353
DP 06	76.2	80	203.2	18.512	0.006	17.231	0.515	1.032
DP 07	76.2	80	203.2	17.990	0.006	16.499	0.635	1.154
DP 08	81.3	65	165.1	23.445	0.040	21.965	0.534	1.331
DP 09	76.2	80	203.2	17.790	0.005	16.463	0.614	0.975
DP 10	63.5	80	203.2	16.883	0.010	15.637	0.468	1.005
DP 11	63.5	65	165.1	13.204	0.001	10.995	0.615	1.878
DP 12	76.2	65	165.1	15.438	0.002	14.026	0.593	1.055
DP 13	63.5	65	165.1	14.019	0.005	12.788	0.495	0.917
Average				17.114	0.013	15.640	0.598	1.142

While minor variation was seen in occupant kinematics and injury criteria values, all simulations followed similar occupant loading conditions. During the oblique impact, the vehicle underwent redirection and rotational motion while the dummy followed its inertia induced initial trajectory towards the A-pillar. The occupant kinematics resulted in harsh initial contact between the dummy head and the roof rail region (Fig.4b). The continued lateral loading of the dummy's head against the roof rail subjected the neck to a compression-flexion loading condition (Fig. 4c-d), leading to peak Nij, before stabilizing for the remainder of the impact event (Fig. 4e-f). This loading condition caused the mean neck injury probability to be the highest whereas all other injury probabilities remained comparatively lower.

This paper is a student paper from the 21st Injury Biomechanics Symposium and is published in a special issue of SAE International Journal of Transportation Safety.
It is preliminary work, has not been peer reviewed, and should not be cited because it is a work in progress.

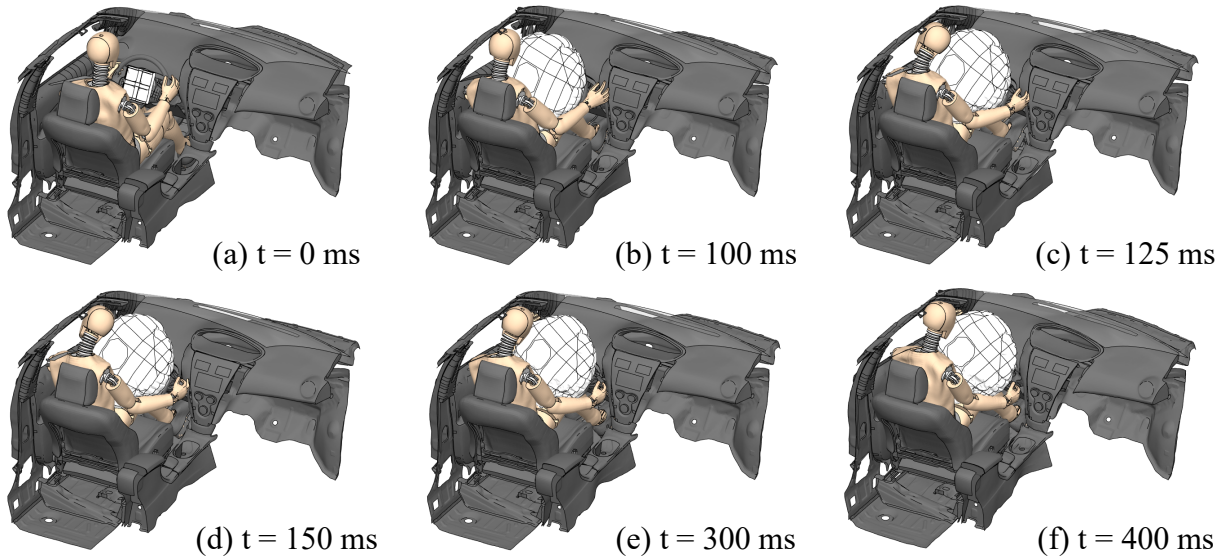

Figure 4: Occupant kinematics and performance during crash simulations.

Sobol Analysis identified hood leading edge height as the most influential geometric parameter affecting injury outcomes. Its influence on full-body, head, neck and chest injury probabilities were determined to be 90.61%, 96.58%, 87.91% and 82.43 respectively (Fig. 5). In contrast, bumper height was most consequential for femur injury probability with 79.95% contribution. However, hood leading edge angle exhibited negligible influence on all injury metrics. The correlation matrix further quantified the direction along with magnitude of relationships between vehicle geometric parameters and injury probabilities, revealing trends consistent with the Sobol analysis. Hood leading edge height demonstrated positive correlation with full-body, head, neck and chest injury probabilities, with coefficients of 0.63, 0.58, 0.61, 0.4 respectively (Fig. 6). Similarly, bumper height positively correlated with femur injury probability (0.47). Similar to the Sobol findings, hood leading edge angle exhibited weak or no correlation with all injury metrics.

Figure 5: Injury probability Sobol analysis for 1100C Small Car (Toyota Yaris).

This paper is a student paper from the 21st Injury Biomechanics Symposium and is published in a special issue of SAE International Journal of Transportation Safety.
It is preliminary work, has not been peer reviewed, and should not be cited because it is a work in progress.

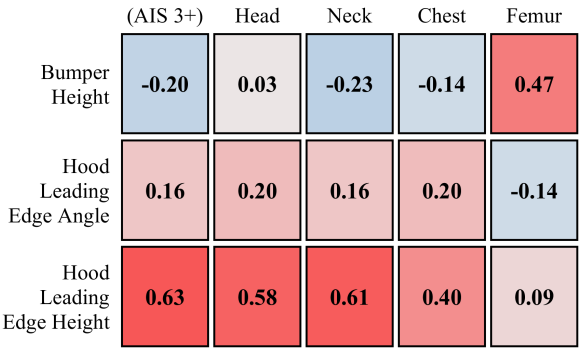

Figure 6: Correlation matrix for 1100C Small Car (Toyota Yaris)

The correlation coefficients are color-coded from blue to red. Blue indicates a strong negative correlation, red a strong positive correlation whereas grey indicates almost no correlation.

DISCUSSION

While the overall performance of the MGS guardrail was satisfactory for all morphed vehicle configurations, geometric variations result in notable vehicle behavior. Designs with a combination of low hood leading edge height and low bumper height exhibited the most pronounced underriding (Fig. 7). Although, no complete underriding similar to that reported in the MwRSF study was observed, several vehicle configurations underwent partial underriding in which the overriding rail approached the base of A-pillar prior to vehicle redirection.

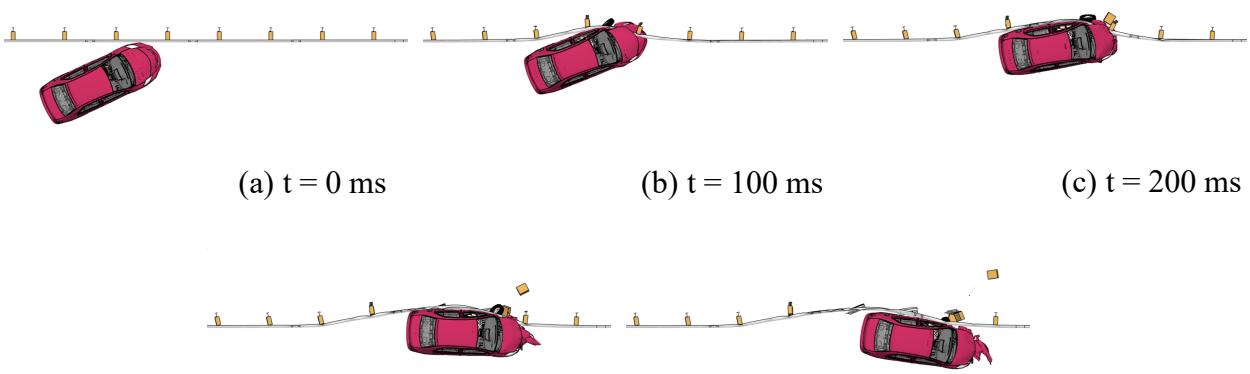

(a) t = 0 ms (b) t = 100 ms (c) t = 200 ms

(d) t = 300 ms (e) t = 400 ms

Figure 7: Vehicle-to-MGS barrier impact simulation conducted according to MASH TL-3 criteria highlighting underriding (DP 01).

These variations in vehicle kinematics help examine the trends identified through the Sobol analysis and correlation assessment between the injury probabilities and the geometric parameters (Fig. 5-6). Increased hood leading edge height was associated with higher probabilities of head,

This paper is a student paper from the 21st Injury Biomechanics Symposium and is published in a special issue of SAE International Journal of Transportation Safety.
It is preliminary work, has not been peer reviewed, and should not be cited because it is a work in progress.

neck, chest, and full body injury risk due to reduced occurrence of underriding. Hood leading edge height determined the pivot point during redirection by influencing the extent of underriding. Configurations exhibiting higher underriding pivoted closer to the occupant compartment, resulting in a reduced lateral acceleration pulse experienced by the occupant during contact with the door panel and a-pillar assembly. In contrast, configurations limited or no underriding pivoted further from the occupant compartment, producing greater lateral loading and correspondingly higher injury probabilities.

Femur injury probability was primarily influenced by bumper height. Increased bumper height was correlated with higher femur injury probability due to its role in determining the initial impact location on the guardrail. Configurations with lower bumper heights directly contacted the guardrail posts during the initial impact, whereas higher bumper heights engaged the W-beam rail. Direct contact with the W-beam produced a more severe longitudinal acceleration pulse, causing earlier and more sever occupant knee interaction with the lower dashboard structure. Conversely, lower bumper heights delayed this engagement due to increased underriding and greater vehicle rotation, which redistributed a portion of the occupant loading into lateral interaction with the door panel.

While this study demonstrated the influence of the front-end geometry on occupant injury risk, several limitations should be acknowledged. A primary limitation was the lack of multiple validated FE models, which necessitated the use of a morphing procedure. Consequently, all the morphed vehicles shared the same underlying structure morphed according to the front-end geometric configuration, unlike real-world vehicle fleet where the underlying structure varies substantially between models. This limitation is particularly relevant when comparing ICEVs with EVs, which lack an engine in the crumple zone. While this restricts the direct generalization of findings, this approach provided the advantage of isolating the sensitivity of front-end geometric parameters. Additional limitations were associated with the vehicle FE model. Since, the FE model was developed based on an older vehicle platform, it was not equipped with a side-curtain airbag. Given the significant lateral loading observed during the oblique impact, the inclusion of modern side-curtain airbags could significantly alter the outcomes. Furthermore, the vehicle had several simplifications, including absence of roof rail paneling which may have increased the severity of head.

CONCLUSIONS

Overall, this investigation concluded that front-end geometric variations influenced vehicle dynamics and the resulting occupant injury criteria. However, no catastrophic barrier failure was observed. Additionally, the dummy-based injury criteria remained within prescribed limits Both observations reiterate the validity of both, MASH test vehicle selection and the flail-space model as a very conservative tool for assessing barrier performance. Consequently, this suggests that factors such as mass and center of gravity height, may play more consequential role in EV-to-barrier interactions.

This paper is a student paper from the 21st Injury Biomechanics Symposium and is published in a special issue of SAE International Journal of Transportation Safety.
It is preliminary work, has not been peer reviewed, and should not be cited because it is a work in progress.

ACKNOWLEDGEMENTS

The authors sincerely appreciate the technical guidance and financial support provided by Insurance Institute of Highway Safety (IIHS). We also acknowledge Midwest Roadside Safety Facility for providing MGS barrier and material models used in this work. Their contributions and valuable assistance significantly enhanced the quality and completion of this work.

REFERENCES

AASHTO. (2016). Manual for assessing safety hardware (MASH). In *American association of state highway transportation officials*.

Alomari, Q. A., Yosef, T. Y., Bielenberg, R. W., Faller, R. K., Negahban, M., Zhang, Z., Li, W., & Humphrey, B. M. (2025). Material Characterization and Stress-State-Dependent Failure Criteria of AASHTO M180 Guardrail Steel: Experimental and Numerical Investigation. *Materials*, *18*(11), 2523.

Andres, A. S. M. R. T., Gatelli, F. C. J. C. D., & Tarantola, M. S. S. (2008). Global sensitivity analysis: the primer. *Ist ed., John Wiley & Sons, The Atrium, Southern Gate, Chichester, England*.

Bandak, F., Eppinger, R., Haffner, M., Khaewpong, N., Kuppa, S., Maltese, M., Nguyen, T., Saul, R., Sun, E., & Takhounts, E. (1999). Development of improved injury criteria for the assessment of advanced automotive restraint systems: II.

Bielenberg, R., Stolle, C., Faller, R., Rosenbaugh, S., Pezzola, G., & Vankirk, J. (2026). Evaluation of the Compatibility of Battery Electric Vehicles With Roadside Hardware. *Transportation Research Record*, *2680*(1), 304-323.

Cassatta, S., Cuddihy, M., Huber, M., Struck, M., Weerappuli, P., & Scavnicky, M. (2013). *Advanced Restraint Systems (ARS) Final Report*.

CEN. (2010a). Road Restraint Systems-Part 2: Performance Classes, Impact Test Acceptance Criteria and Test Methods for Safety Barriers. In *European Committee for Standardization;* .

CEN. (2010b). Road Restraint Systems-Part 3: Performance Classes, Impact Test Acceptance Criteria and Test Methods for Crash Cushions. In *European Committee for Standardization;* .

CEN. (2010c). Road restraint systems part 1: terminology and general criteria for test methods (EN 1317-1). In: European Committee for Standardization Brussels.

Eigen, A. M., & Glassbrenner, D. (2004). *The relationship between occupant compartment deformation and occupant injury*.

Eppinger, R., Kuppa, S., Saul, R., & Sun, E. (2000). Supplement: development of improved injury criteria for the assessment of advanced automotive restraint systems: Ii.

Ferdous, M. R., Abu-Odeh, A., Bligh, R. P., Jones, H. L., & Sheikh, N. M. (2011). Performance limit analysis for common roadside and median barriers using LS-DYNA. *International Journal of Crashworthiness*, *16*(6), 691-706.

Gandikota, I., Rais-Rohani, M., DorMohammadi, S., & Kiani, M. (2015). Multilevel vehicle–dummy design optimization for mass and injury criteria minimization. *Proceedings of the*

This paper is a student paper from the 21st Injury Biomechanics Symposium and is published in a special issue of SAE International Journal of Transportation Safety.
It is preliminary work, has not been peer reviewed, and should not be cited because it is a work in progress.

Institution of Mechanical Engineers, Part D: Journal of automobile engineering, *229*(3), 283-295.
Gennarelli, T. A., & Wodzin, E. (2006). AIS 2005: a contemporary injury scale. *Injury*, *37*(12), 1083-1091.
Hu, W., Monfort, S. S., & Cicchino, J. B. (2024). The association between passenger-vehicle front-end profiles and pedestrian injury severity in motor vehicle crashes. *Journal of safety research*, *90*, 115-127.
Julin, R. D., Reid, J. D., Faller, R. K., & Mongiardini, M. (2012). *Determination of the Maximum MGS Mounting Height–Phase II Detailed Analysis Using LS-DYNA®*.
Kang, S., Chen, C., Guha, S., Paladugu, M., Ramasamy, M. S., Gade, L., & Zhu, F. (2018). LS-DYNA® belted occupant model. 15th International LS-DYNA Users Conference,
Kuppa, S., Rupp, J., & Schneider, L. (2000). Knee-Thigh-Hip Injuries and Knee/Femur compliance of the Hybrid III, Thor-Lx, and Human cadavers. In: NHTSA.
Kuppa, S., Wang, J., Haffner, M., & Eppinger, R. (2001). *Lower extremity injuries and associated injury criteria*.
Liu, C., Boothman, S. G., & Graham, J. D. (2025). The rise and recent decline of Tesla's share of the US electric vehicle market. *World Electric Vehicle Journal*, *16*(2), 90.
Marzougui, D., Mohan, P., & Kan, S. (2007). *Evaluation of rail height effects on the safety performance of W-beam barriers*.
Masiá, J., Eixerés, B., & Dols, J. (2008). Models for airbag simulation in vehicles adapted for disabled drivers. *Zaragoza*.
Meng, Y., Buckland, E., & Untaroiu, C. (2026). Numerical investigation of driver injury risks in car-to-end terminal crashes using a human finite element model. *Computer methods in biomechanics and biomedical engineering*, *29*(1), 245-255.
Michie, J. D. (1981). *Collision Risk Assessment Based on Occupant Flail Space Model*. The Institute.
Nason, N. (2007). Petition for Rulemaking Regarding Federal Motor Vehicle Safety Standard No. 208 (49 CFR 571.208) Occupant Crash Protection.
NHTSA. (2023). Federal Motor Vehicle Safety Standard No. 208: Occupant Crash Protection. In. 49 CFR §571.208, U.S. Department of Transportation: National Highway Traffic Safety Administration.
Noureddine, A., Eskandarian, A., & Digges, K. (2002). Computer modeling and validation of a hybrid III dummy for crashworthiness simulation. *Mathematical and computer modelling*, *35*(7-8), 885-893.
Pearson, K. (1895). VII. Note on regression and inheritance in the case of two parents. *proceedings of the royal society of London*, *58*(347-352), 240-242.
Polivka, K. A., Faller, R. K., Sicking, D. L., Rohde, J. R., Bielenberg, R. W., & Reid, J. D. (2006). Performance Evaluation of the Midwest Guardrail System–Update to NCHRP 350 Test No. 3-11 with 28" CG Height (2214MG-2).
Polivka, K. A., Sicking, D. L., Rohde, J. R., Faller, R. K., Reid, J. D., Holloway, J. C., & Kuipers, B. D. (2004). Developments of the midwest guardrail system for standard and reduced post spacing and in combination with curbs.
Ray, M. H., Mongiardini, M., Plaxico, C. A., & Anghileri, M. (2011). *Procedures for verification and validation of computer simulations used for roadside safety applications*.

This paper is a student paper from the 21st Injury Biomechanics Symposium and is published in a special issue of SAE International Journal of Transportation Safety.
It is preliminary work, has not been peer reviewed, and should not be cited because it is a work in progress.

Storozhev, S. A., & Vafaeva, K. M. (2025). Crashworthiness of existing bridge guardrails for heavier electric vehicles: An analysis of barrier deformation. *Construction of Unique Buildings and Structures*, *118*(4), 11806-11806.

Yücel, A. Ö. (2024). Impact of electric cars on the crash performance of longitudinal barriers. *Kahramanmaraş Sütçü İmam Üniversitesi Mühendislik Bilimleri Dergisi*, *27*(2), 488-501.

Żuchowski, A. (2018). Results of the crash tests of electric cars. *Journal of KONES*, *25*(1), 483-490.

This paper is a student paper from the 21st Injury Biomechanics Symposium and is published in a special issue of SAE International Journal of Transportation Safety.
It is preliminary work, has not been peer reviewed, and should not be cited because it is a work in progress.